

# Large-scale JPEG steganalysis using hybrid deep-learning framework

Jishen Zeng, Shunquan Tan\*, Member, IEEE, Bin Li, Member, IEEE, and Jiwu Huang, Fellow, IEEE

**Abstract**—Deep learning frameworks have achieved overwhelming superiority in many fields of pattern recognition in recent years. However, the application of deep learning frameworks in image steganalysis is still in its initial stage. In this paper we firstly proved that the convolution phase and the quantization & truncation phase are not learnable for deep neural networks. Then on the basis of the theoretical analysis, we proposed a new hybrid deep-learning framework for JPEG steganalysis, which is made up of two hybrid parts. The first part is hand-crafted. It corresponds to the convolution phase and the quantization & truncation phase of the rich models. The second part is a compound deep neural network containing three CNN subnets in which the model parameters are learnable during the training procedure. We have conducted extensive experiments on large-scale dataset extracted from ImageNet. Primary dataset used in our experiments contains one million images, while our largest dataset contains ten million images. The large-scale experiments show that our proposed framework outperforms all other steganalytic models (hand-crafted or deep-learning based) in the literature. Furthermore, the experimental results revealed that our proposed framework possesses some great features, including well attacking-target transfer ability and insensitive to altered JPEG block artifact.

**Index Terms**—hybrid deep-learning framework, CNN network, steganalysis, steganography.

## I. INTRODUCTION

**S**TEGANOGRAPHY is the art of covert communications. As the adversary of steganography, steganalysis focuses on developing methods for detecting the presence of secret messages concealed by steganography [1]. In the digital era, digital images are among the most ideal cover works due to the fact that they are easy to acquire and widely distributed in the internet. As a result, digital image steganography and steganalysis has become a research hotspot in the field of information security in recent years.

Digital image steganography can be divided into two categories: spatial-domain image steganography and frequency-domain image steganography. The de facto sole frequency-domain image steganography is JPEG image steganography, which keeps attracting great scholarly attention in recent years. In both categories, almost all of the state-of-the-art steganographic algorithms adopt content-adaptive embedding schemes [2], [3]. Most of these schemes use an additive

This work was supported in part by the NSFC (61332012, 61402295, 61572329), Guangdong NSF (2014A030313557). (Corresponding author: Shunquan Tan.)

S. Tan is with College of Computer Science and Software Engineering, Shenzhen University. J. Zeng, B. Li, and J. Huang are with College of Information Engineering, Shenzhen University.

All the members are with Shenzhen Key Laboratory of Media Security, Guangdong Province, 518060 China. (e-mail: tansq@szu.edu.cn).

distortion function defined as the sum of costs of all changed elements. From early HUGO [4] and WOW [5], to latest HILL [6], [7], MVG [8] and MiPOD [9], the past few years witness the flourish of additive schemes in spatial domain. In JPEG domain, UED [10] and UERD [11] are two additive schemes with good security. UNIWARD proposed by Holub et al. [12] is an additive distortion function which can be applied for embedding in spatial domain and JPEG domain. Its JPEG version, J-UNIWARD outperforms other state-of-the-art JPEG steganographic algorithms [11], [12]. Research on non-additive distortion functions has made great progress in spatial domain [13], [14]. However, no non-additive scheme has been proposed in JPEG domain, as far as we know. Although utilizing side information of a pre-cover image (raw or uncompressed) can improve the security of JPEG steganography [11], [12], side-informed JPEG steganography is not desirable for practical applications since pre-cover images are scarce compared with handy JPEG format covers.

Steganalysis, on the other hand, has evolved from early targeted steganalytic algorithms [15], [16] into universal steganalytic frameworks. Most of modern universal steganalytic detectors are the combination of a rich model that include tens of thousands of features [17]–[20] and an ensemble classifier [21]. In spatial domain, SRM [17] and its selection-channel-aware variants [18]–[20] reign supreme. In JPEG domain, DCTR [22] is a steganalytic features set with relatively low dimensionality and competitive performance. PHARM proposed by Holub et al. [23] exhibits better performance, although with higher dimensionality w.r.t. DCTR. In [24], Denemark et al. proposed SCA, a selection-channel-aware variant of JPEG rich models, e.g. DCTR and PHARM, targeted at content-adaptive JPEG steganography<sup>1</sup>.

In recent years, with help of parallel computing ability provided by GPGPU (general-purpose computing on graphics processing units) and huge amounts of training data, deep learning frameworks have achieved overwhelming superiority over conventional approaches in many fields of pattern recognition and machine learning [25]. The researchers in image steganalysis have also started to invest effort in applying deep learning frameworks to this field [26]–[30]. In [26], Tan and Li firstly explored the application of stacked convolutional auto-encoders, a specific form of deep learning frameworks in image steganalysis. In [27], Qian et al. proposed a steganalyzer based on CNN (convolutional neural network), whose performance is close to SRM. In [28], Pibre et al.

<sup>1</sup>The acronyms listed here for the steganographic and steganalytic algorithms are taken from the original papers. The corresponding full names are omitted for brevity.

revealed that CNN based steganalyzer can achieve superior performance when there are fixed modification patterns in stego images. In [29], [30], Xu et al. constructed another CNN based steganalyzer equipped with BN (batch normalization) layers. Its performance surpass SRM. However, like their rich-model-based competitors [17]–[20], [22]–[24], the above approaches [26]–[30] are all focus on spatial-domain steganalysis and are all evaluated on BOSSBase (v1.01), a small-scale image database [31]. BOSSBase (v1.01) is by far the de facto benchmarking image dataset in the field of steganography and steganalysis. Whereas with only 10,000 images BOSSBase is argued to be not an adequate representative of real-world steganalysis performance [32]. None of them addresses the application of deep learning frameworks in JPEG domain steganalysis, which does not match the widespread use of JPEG images.

In this paper, we firstly proved that the two crucial components of rich models, the convolutional kernels used to extract diverse noise residuals and the threshold quantizers used to reduce model complexity can not be efficiently learned by deep-learning frameworks. Based on the theoretical analysis, we proposed a hybrid deep-learning framework for large-scale JPEG steganalysis. It is the assembly of the bottom hand-crafted diverse convolutional-kernels & threshold-quantizers pairs and the upper compact deep-learning models. Extensive experiments conducted on ImageNet [33], a large-scale image dataset which contains more than fourteen million JPEG images show that the performance of our proposed framework is far superior to both rich-model-based steganalyzers and other deep-learning-based steganalyzers in the literature. Furthermore, the proposed hybrid deep-learning framework exhibits good properties, including good transfer ability among different steganographic algorithms, performance stability among different scales of datasets, and insensitivity of the impact of JPEG block artifact.

The rest of the paper is organized as follows. Sect. II firstly provides a theoretical foundation of our proposed approach and then describes our proposed hybrid deep-learning framework in details. Results for experiments conducted on ImageNet dataset are presented in Sect. III. Finally, we conclude the proposed approach in Sect. IV.

## II. HYBRID DEEP-LEARNING FRAMEWORK FOR LARGE-SCALE JPEG STEGANALYSIS

### A. Preliminaries

State-of-the-art JPEG rich-model based steganalytic algorithms [22]–[24] take decompressed JPEG images as input. Like their spatial-domain companions, the feature extraction procedure of JPEG rich models can be divided into three phases:

- *Convolution*: The target image is convolved with a set of kernel matrices to generate diverse types of noise residuals. The purpose of this phase is to suppress the image contents as far as possible.
- *Quantization and truncation* (Q&T for short): Different quantized and truncated versions of each residual are

calculated to further improve the diversity of the resulting features, as well as reduce the computational complexity.

- *Pooling*: Aggregation of the values in noise residuals to further reduce feature dimensions and generate the final rich-model steganalytic feature set.

Take DCTR [22] for example. Given a  $M \times N$  JPEG image, it is firstly decompressed to the corresponding spatial-domain version  $\mathbf{X} \in \mathbb{R}^{M \times N}$ . Sixty-four  $8 \times 8$  DCT basis patterns are defined as  $\mathbf{B}^{(k,l)} = (B_{mn}^{(k,l)})$ ,  $0 \leq k, l \leq 7, 0 \leq m, n \leq 7$ :

$$B_{mn}^{(k,l)} = \frac{w_k w_l}{4} \cos \frac{\pi k(2m+1)}{16} \cos \frac{\pi l(2n+1)}{16}, \quad (1)$$

where  $w_0 = \frac{1}{\sqrt{2}}$ ,  $w_k = 1$  for  $k > 0$ .  $\mathbf{X}$  is convolved with  $\mathbf{B}^{(k,l)}$  to generate 64 noise residuals  $\mathbf{U}^{(k,l)}$ ,  $0 \leq k, l \leq 7$ :

$$\mathbf{U}^{(k,l)} = \mathbf{X} * \mathbf{B}^{(k,l)}, \quad (2)$$

Then the elements in each  $\mathbf{U}^{(k,l)}$  are quantized with a pre-defined quantization step  $q$  and then truncated with a given threshold  $T$ . The DCTR features are built by a particular pooling operation, namely collecting a specific first-order statistic separately for the absolute values of the quantized and truncated elements in each  $\mathbf{U}^{(k,l)}$ .

In [26], we have already pointed out that by virtue of the structure, rich steganalytic models exhibit similarity to CNN. CNN is a cascade of alternating convolutional layers, regulation layers (e.g. BN layers) and pooling layers. Regardless of the types of the layers, they are made up of units that have learnable weights and biases. Each unit receives inputs from some units of a previous layer, performs a dot product with weights and optionally follows it with a nonlinear point-wise activation function. CNN can be trained using backpropagation algorithm. Denote the cascade of layers in a given CNN as  $[L_1, L_2, \dots, L_n]$ , in which  $L_1$  is the input layer while  $L_n$  is the output layer. Let  $a_i^{(l)}$  denote the activation (output) of unit  $i$  in layer  $L_l$ . For  $L_1$ ,  $a_i^{(1)}$  denotes the  $i$ -th input.  $W_{ij}^{(l)}$  denotes the weight associated with unit  $i$  in  $L_l$  and unit  $j$  in  $L_{l+1}$ , while  $b_j^{(l)}$  denotes the bias associated with unit  $j$  in  $L_{l+1}$ .  $z_j^{(l+1)}$  denotes the weighted sum of inputs to unit  $j$  in  $L_{l+1}$ :

$$z_j^{(l+1)} = \sum_i W_{ij}^{(l)} a_i^{(l)} + b_j^{(l)} \quad (3)$$

and  $a_j^{(l+1)} = f(z_j^{(l+1)})$  in which  $f(\cdot)$  denotes the activation function. Denote the set of all  $W_{ij}^{(l)}$  and  $b_j^{(l)}$  in a neural network as  $W$  and  $b$ , respectively.  $W$  and  $b$  constitute the parameter set of a neural network. For a mini-batch of training features-label pairs  $\{(x^{(1)}, y^{(1)}), \dots, (x^{(m)}, y^{(m)})\}$ , the goal of backpropagation algorithm is to minimize  $J(W, b)$  which denotes the overall cost function with respect to  $W$  and  $b$ :

$$J(W, b) = \frac{1}{m} \sum_{h=1}^m J(W, b; x^{(h)}, y^{(h)}) + R(W) \quad (4)$$

in which  $R(W)$  is the regularization term and  $J(W, b; x^{(h)}, y^{(h)})$  is the error metric with respect to a single example  $(x^{(h)}, y^{(h)})$ . To achieve this goal, for each training sample backpropagation algorithm firstly performs a feedforward pass and computes the activations for layers  $L_2, L_3$  and so on up to the output layer  $L_n$ . Then it performs a backpropagation pass in which from

the output layer  $L_n$  down to the second last layer  $L_2$  the partial derivatives with respect to  $W_{ij}^{(l)}$  and  $b_j^{(l)}$ ,  $l = n, n-1, \dots, 2$  are calculated as:

$$\begin{cases} \frac{\partial}{\partial W_{ij}^{(l)}} J(W, b; x^{(h)}, y^{(h)}) = a_i^{(l)} \vartheta_j^{(l+1)} \\ \frac{\partial}{\partial b_j^{(l)}} J(W, b; x^{(h)}, y^{(h)}) = \vartheta_j^{(l+1)} \end{cases} \quad (5)$$

where

$$\begin{cases} \vartheta_j^{(n)} = \frac{\partial}{\partial a_j^{(n)}} J(W, b; x^{(h)}, y^{(h)}) f'(z_j^{(n)}) \\ \vartheta_j^{(l)} = (\sum_k W_{jk}^{(l)} \vartheta_k^{(l+1)}) f'(z_j^{(l)}) \end{cases} \quad (6)$$

Gradient descent algorithm is used to find the optimal  $W$  and  $b$ . In the optimization procedure, it updates  $W$  and  $b$  according to steps proportional to the negative of the average of  $m$  gradients each of which is the vector whose components are the partial derivatives in (5) [34].

### B. Theoretical analysis

Although rich steganalytic models exhibit similarity to CNN, in former researches it has been observed that CNN is hard to learn some core components in rich models, especially the specific kernel matrices in convolutional operation of rich models [26]–[28]. However as far as we know, no theoretical analysis is made for this phenomenon. In the following propositions, we show that not only the convolution phase but also the Q&T phase of rich models are not learnable for CNN.

#### Proposition 1.

- 1) *The kernel matrices used to generate noise residuals in rich models can not be evolved from the randomly initialized kernels of a convolutional layer in CNN. This problem is unsolvable even with traditional data preprocessing strategies.*
- 2) *Better performing kernels can not be evolved from the kernels possessing the same parameters as those used in rich models, provided the model is trained with gradient descent algorithm.*

*Proof:* In the contexts of steganography and steganalysis, an input image can be represented as  $\mathbf{X} = (x_{pq}) = \mathbf{C} + \mathbf{N}$ , where  $\mathbf{C} = (c_{pq}) \in [0, 255]^{M \times N}$  denotes the corresponding grayscale cover image. When  $\mathbf{X}$  is a stego image,  $\mathbf{N} = (n_{pq}) \in \{-1, 0, 1\}^{M \times N}$  denotes the zero mean stego noise if a ternary embedding scheme is adopted in steganography. When  $\mathbf{X}$  is an innocent cover image,  $\mathbf{N}$  is a zero matrix.

Suppose that we want to train a convolutional layer with kernels of size of  $m \times n$  to generate noise residuals, it should be located at the second layer of the CNN hierarchy. Please note that the convolution in a convolutional layer is just one sort of representation of the dot product with local-connected-and-shared weights. As a result, from (3), let  $l = 2$ , replace the one-dimensional index with two-dimensional index used in a convolutional layer and restrict the size of the dot product to

$m \times n$ , we can get:

$$\begin{aligned} z_j^{(2)} &= \sum_{p=1}^M \sum_{q=1}^N W_{pq,j}^{(1)} a_{pq}^{(1)} + b_j^{(1)} = \sum_{p=1}^m \sum_{q=1}^n W_{pq,j}^{(1)} a_{pq}^{(1)} + b_j^{(1)} \\ &= \sum_{p=1}^m \sum_{q=1}^n W_{pq,j}^{(1)} x_{pq} + b_j^{(1)} = \sum_{p=1}^m \sum_{q=1}^n W_{pq,j}^{(1)} (c_{pq} + n_{pq}) + b_j^{(1)} \\ &= \sum_{p=1}^m \sum_{q=1}^n W_{pq,j}^{(1)} c_{pq} + \sum_{p=1}^m \sum_{q=1}^n W_{pq,j}^{(1)} n_{pq} + b_j^{(1)} \\ &\approx \sum_{p=1}^m \sum_{q=1}^n W_{pq,j}^{(1)} c_{pq} + b_j^{(1)} \end{aligned} \quad (7)$$

(7) is hold due to the fact that the convolutional layer is fed with input images therefore  $a_{kl}^{(1)} = x_{kl}$ , and by average  $|c_{pq}|$  is two orders of magnitude larger than  $|n_{pq}|$ . According to (5) and (6) we can see that in one iteration of backpropagation, when the gradient is backpropagated to  $L_2$ ,  $\frac{\partial}{\partial W_{jk}^{(2)}} J(W, b; x^{(h)}, y^{(h)}) \propto a_j^{(2)}$  since  $\vartheta_k^{(3)}$  is fixed. Then  $a_j^{(2)} \propto z_j^{(2)}$  due to the fact that all of the commonly used activation functions, including Sigmoid, TanH and ReLU are monotonic increasing. As a result  $\frac{\partial}{\partial W_{jk}^{(2)}} J(W, b; x^{(h)}, y^{(h)}) \propto z_j^{(2)}$ . According to (7), the influence of stego noise  $\mathbf{N}$  to  $\frac{\partial}{\partial W_{jk}^{(2)}} J(W, b; x^{(h)}, y^{(h)})$  can be neglected. Therefore gradient descent algorithm will be guided by the cover image contents rather than the stego noise. No explicit guidelines to supervise gradient descent algorithm to suppress cover image contents at the same time strengthen stego noise. As a result, the kernel matrices used to generate noise residuals in rich models can not be evolved from the CNN convolutional kernels.

Furthermore, since during the training procedure stego noise is mixed with image contents, traditional data preprocessing strategies, including mean subtraction, normalization, and whitening cannot narrow the gap of the order of magnitude between  $|c_{pq}|$  and  $|n_{pq}|$ . Thus data preprocessing strategies cannot help resolving the problem. The proof of Part 1) is obtained.

Since the proof is irrelevant to the initial state of the kernels of the corresponding convolutional layers. Thus the influence of  $\{n_{pq}\}$  to  $\frac{\partial}{\partial W_{jk}^{(2)}} J(W, b; x^{(h)}, y^{(h)})$  still can be neglected even trained from the convolutional kernels possessing the same parameters as those used in rich models. Therefore the proof of Part 2) is also obtained. ■

#### Proposition 2.

- 1) *The Q&T non-linearity saturates and kills gradients so that can not be put in the pipeline of gradient descent.*
- 2) *The Q&T in rich models can be neither evolved from commonly used activation functions in CNN, nor imitated by a cascade of layers in CNN.*

*Proof:* The Q&T in rich models takes noise residuals generated by kernel matrices as input. They can be modeled as:

$$a_j^{(2)} = f(z_j^{(2)}) = \begin{cases} \min([z_j^{(2)}/q], T) & \text{if } z_j^{(2)} \geq 0 \\ \max([z_j^{(2)}/q], -T) & \text{if } z_j^{(2)} < 0 \end{cases} \quad (8)$$

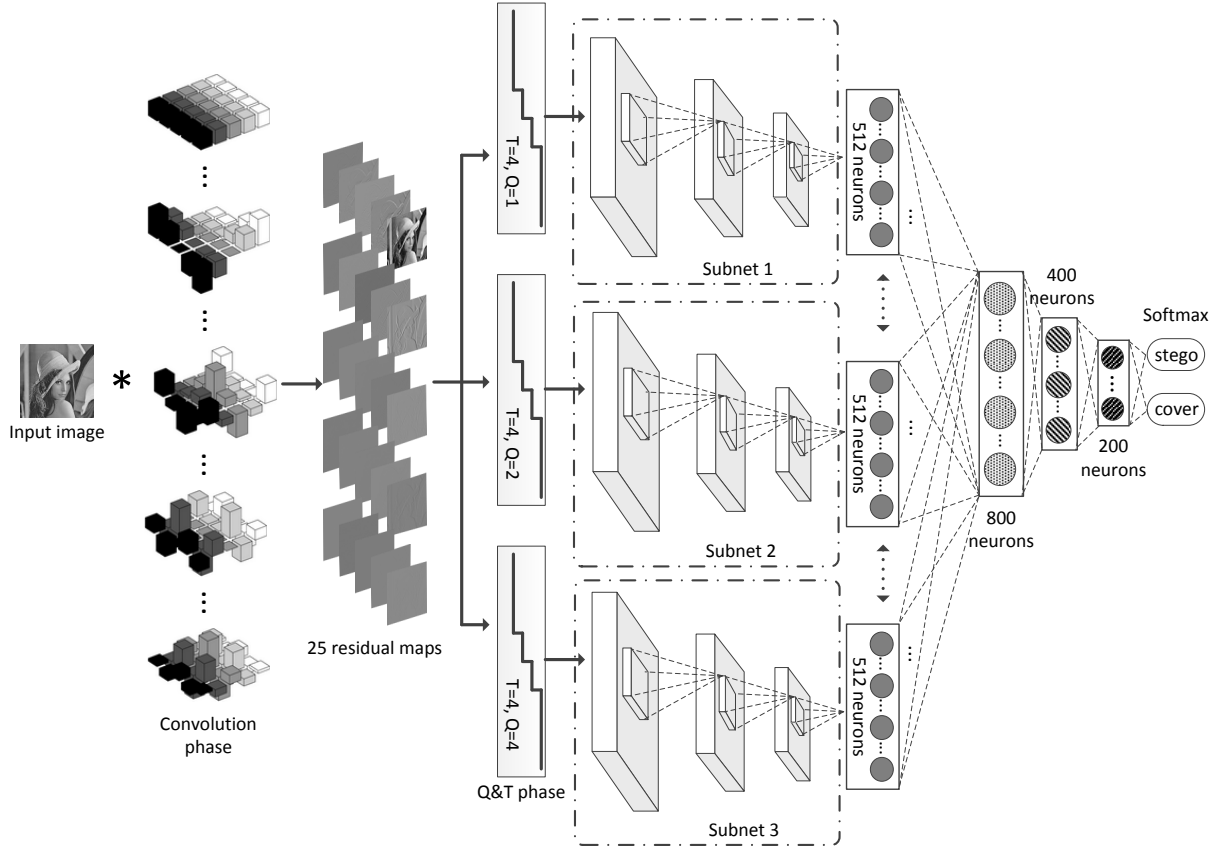


Fig. 1. The conceptual architecture of our proposed hybrid deep-learning framework. Given an input image (the LENA image is used here for demonstration), it is convolved with  $5 \times 5$  DCT basis patterns to generate twenty-five corresponding residual maps. The residual maps are separately quantized and truncated with three different threshold quantizers. The central part of our proposed hybrid deep-learning framework are three parallel CNN subnets. Each of them takes one quantized and truncated residual map as input, respectively. The features generated by them are concatenated together. Another three-layer fully-connected neural network is built upon them to output the final prediction.

where  $z_j^{(2)}$  is an element of a given noise residual,  $a_j^{(2)}$  is the corresponding activation output,  $q$  is the quantization step,  $\lfloor \cdot \rfloor$  denotes the rounding operation, and  $T$  is a predefined threshold. (8) can be rewritten as a staircase function:

$$f(z_i^{(2)}) = \sum_{k=-T}^T k \cdot \chi_{A_k}(z_i^{(2)})/q \quad (9)$$

where  $k \in \mathbb{Z}$ ,  $\chi_{A_k}$  is an indicator function of  $A_k$  and  $\{A_k\}$  is a union of intervals:

$$A_k = \begin{cases} (-\infty, T + 0.5], & k = -T \\ (k - 0.5, k + 0.5], & -T < k < 0 \\ (-0.5, 0.5), & k = 0 \\ [k - 0.5, k + 0.5], & 0 < k < T \\ [T - 0.5, +\infty), & k = T \end{cases} \quad (10)$$

Therefore the derivative:

$$f'(z_j^{(2)}) = \frac{da_j^{(2)}}{dz_j^{(2)}} = \sum_{k=-T}^T k \cdot \delta\left(\frac{z_j^{(2)}}{q} - k + 0.5\right) \quad (11)$$

where  $\delta(\cdot)$  is the Dirac delta function which is zero everywhere except at zero point is infinite. As a result  $f'(z_j^{(2)})$  is zero along the entire domain of  $z_j^{(2)}$  except the set of points  $\{-T + 0.5, -T + 1.5, \dots, T - 1.5, T - 0.5\}$ . According to (6) we can see that if (8) is used as the activation function, the

partial derivative it passes on will become infinite, namely no derivative if  $z_i^{(2)}$  is located at each point of the set  $\{-T + 0.5, -T + 1.5, \dots, T - 1.5, T - 0.5\}$ , otherwise zero. The corresponding gradient saturates if the partial derivative it passes on approaches to zero, and is killed if there is no derivative. Thus the proof of Part 1) is obtained. Likewise, when a cascade of layers in CNN try to learn a staircase function represented in (9) the backpropagation will get stuck since the corresponding partial derivatives transmitted in the layers will approach to zero or infinite. Thus the proof of Part 2) is also obtained. ■

### C. Our proposed hybrid deep-learning framework

According to the theoretical analysis in Sect. II-B, we propose a hybrid deep-learning framework whose conceptual architecture is illustrated in Fig. 1. The proposed framework is composed of two parts. The first part corresponds to the convolution phase and the Q&T phase of the rich models. More specifically, this part of our framework incorporated the first two phases of DCTR [22]. All the model parameters in this part are hand-crafted and gradient-descent-based learning is disabled. What makes this part different from DCTR is that DCTR uses sixty-four  $8 \times 8$  DCT basis patterns and only one Q&T combination, while the first part of our proposed

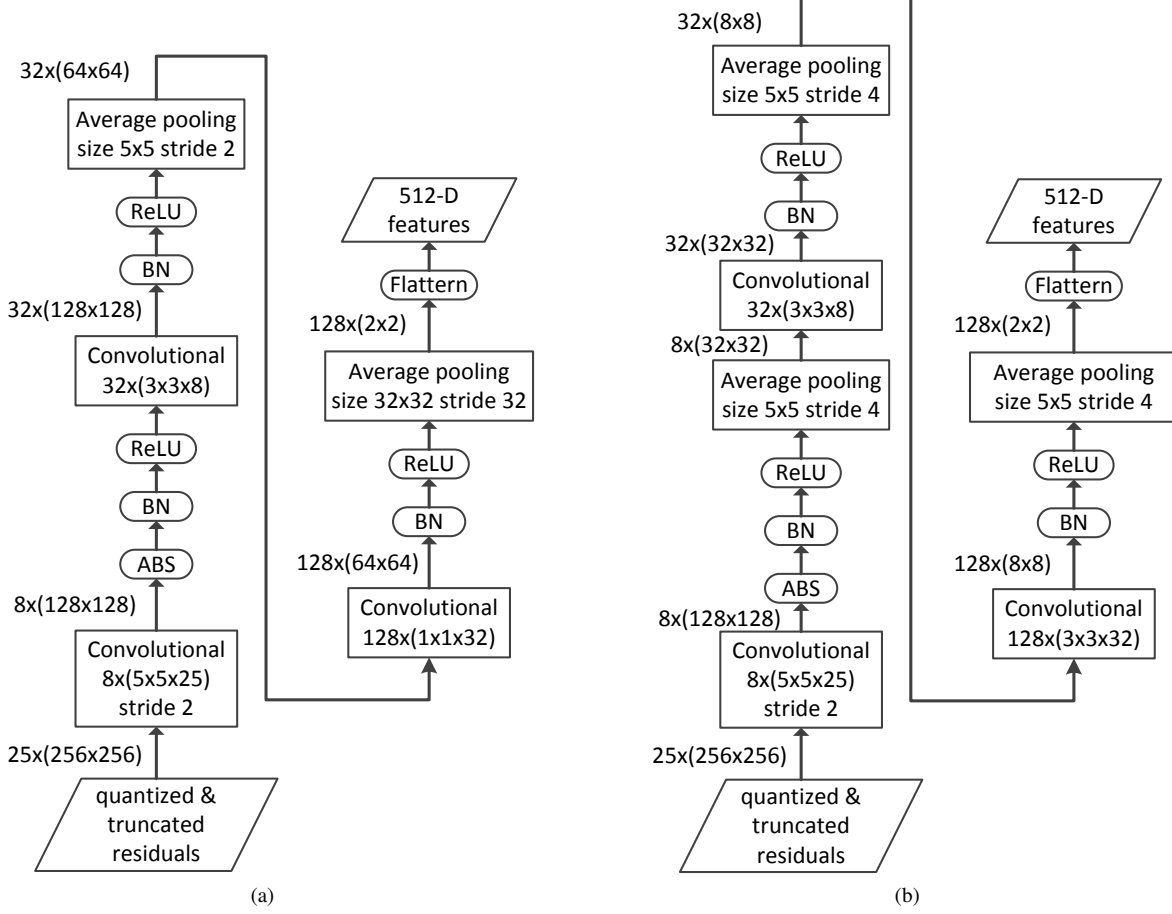


Fig. 2. Two types of subnet configurations. (a) A simplified configuration modified from the framework proposed by Xu et al. [29]. (b) A traditional configuration with progressive pooling layers and top-level convolutional kernels larger than 1x1.

framework contains twenty-five 5x5 DCT basis patterns which are defined as  $\mathbf{B}^{(k,l)} = (B_{mn}^{(k,l)})$ ,  $0 \leq k, l \leq 5$ ,  $0 \leq m, n \leq 5$ :

$$B_{mn}^{(k,l)} = \frac{w_k w_l}{4} \cos \frac{\pi k(2m+1)}{10} \cos \frac{\pi l(2n+1)}{10},$$

$$w_0 = \frac{1}{\sqrt{2}}, \quad w_k = 1 \text{ for } k > 0. \quad (12)$$

and three Q&T combinations, namely ( $T = 4, Q = 1$ ), ( $T = 4, Q = 2$ ) and ( $T = 4, Q = 4$ ). Given an input image, the convolution phase outputs twenty-five residual maps. The residual maps pass through the Q&T phase. Three different groups of quantized and truncated residual maps are generated. They constitute the input of the second part.

The second part is a compound deep CNN network in which the model parameters are learnable during the training procedure. The bottom of the second part contains three independent subnets with identical structures. Each one of the subnets corresponds to one group of quantized and truncated residual maps. They take the residual maps as input and generate three feature vectors, respectively. As shown in Fig. 2, two types of subnet configurations are adopted in our proposed framework. Both of them contain three convolutional layers and output 512-D (512 dimensional) feature vector. The first one, denoted as *type1* (Fig. 2(a)) is a simplified configuration

modified from the framework proposed by Xu et al. [29]<sup>2</sup>. The second one, denoted as *type2* (Fig. 2(b)) is a traditional CNN configuration. Compared with the first configuration, it adopts progressive pooling layers and replaces the unusual 1x1 convolutional kernels in the top-most convolutional layer with traditional 3x3 kernels. With progressing pooling layers, *type2* subnet is a relative GPU memory conservation model. The GPU memory requirement of *type2* is only one-seventh of that of *type1*. Both of the configurations have in common are the BN layers which follow every convolutional layers.

The three 512-D feature vectors outputted by the bottom subnets are concatenated together to generate a single 1536-D feature vector, which is then fed into a top four-layer fully-connected neural network to output the final prediction. The first layer of the fully-connected neural network consist of 800 neurons, the second layer consist of 400 neurons, while the third layer consist of 200 neurons. ReLU activation functions are used in all of the three layers. The top layer contains two neurons which denote “stego” prediction and “cover” prediction, respectively. Softmax function is used to output

<sup>2</sup>Two convolutional layers and the corresponding affiliated ones, a.k.a. “Group 2” and “Group 4” in Xu’s model are removed. Some layer parameters are altered accordingly. The dimension of the output feature vector is changed from 128-D to 512-D.

probabilities of the two predictions.

State-of-the-art deep-learning researches revealed that ensemble prediction with independently trained deep-learning models can significantly improve the performance [35]. We also bring in model ensemble in the final prediction. Five versions of our proposed deep-learning models are independently trained. When testing, ensemble predictions (majority voting) are performed with them.

In a nutshell, the basic concepts behind our proposed hybrid deep-learning framework are listed as follow:

- 1) We approve the concepts behind rich models [17] that model diversity is crucial to the performance of steganalytic detectors. The model diversity of our proposed framework is represented in twenty-five DCT basis patterns in the hand-crafted convolutional layer and the three Q/T combinations that followed. There are total  $25 \times 3 = 75$  sub-models in our proposed framework.
- 2) We believe that as pointed out in [29], [36], batch normalization is an efficient regularizer to boost the performance of our proposed framework. As a result, BN layers are inserted following the convolutional layers for both the configurations of the subnets in Fig. 2.
- 3) We believe that under the same depth condition, the subnet CNN models with intermediate feature maps larger in size should retain more information useful for model learning, although with the cost of GPU memory consumption. Therefore our proposed framework with type1 subnet should behave better than that with type2 subnet.
- 4) We believe that ensemble of independently trained models based on our proposed framework can boost the steganalytic performance and further eliminate the performance difference between different configurations of the subnets.

All of the above concepts are verified in our extensive experiments, as shown in Sect. III.

### III. EXPERIMENTAL RESULTS

#### A. Experiment setups

We adopt ImageNet [33], a large-scale image dataset which contains more than fourteen million JPEG images to evaluate the steganalytic performance of our proposed hybrid deep-learning framework. All of the experiments are conducted on a GPU cluster with eight NVIDIA® Tesla® K80 GPU cards. Based on machine capacity considerations, we restrict the size of the target images to  $256 \times 256$ . 50K, 500K and 5,000K JPEG images with size larger than  $256 \times 256$  are randomly picked out from ImageNet. Their left-top  $256 \times 256$  regions are cropped, greyed and then JPEG re-compressed with quality factor 75. The resulting images constitute the following three basic cover image datasets:

- basic50K: Mainly used for small-scale verification experiments to determine hyper-parameters of our proposed framework.
- basic500K: The major dataset for most all of our experiments.

TABLE I  
EFFECT OF DIFFERENT Q/T COMBINATIONS, DIFFERENT HAND-CRAFTED CONVOLUTIONAL KERNELS, AND THE PRESENCE OF BN LAYERS. THOSE ADOPTED IN OUR PROPOSED FRAMEWORK ARE MARKED WITH RECTANGLES. LOGOGRAMS ARE USED IN EXPRESSING Q/T COMBINATIONS. FOR EXAMPLE, (4,1) DENOTES  $(T = 4, Q = 1)$ . THE BEST RESULTS IN EVERY SUB-TABLES ARE UNDERLINED.

Quantization Steps & Threshold	BN Layers		
	With All	Without BN1	Without All
<b>Nine <math>3 \times 3</math> DCTR kernels</b>			
(4, 1), (4, 1.5), (4, 2)	73.1%	70.6%	50.1%
(4, 2), (4, 2), (4, 2)	72.8%	70.1%	50.0%
(4, 1), (4, 2), (4, 4)	<u>73.2%</u>	71.0%	50.1%
(2, 1), (4, 2), (6, 4)	71.2%	68.5%	50.0%
(6, 1), (4, 2), (2, 4)	70.6%	67.8%	50.0%
<b>Twenty-five <math>5 \times 5</math> DCTR kernels</b>			
(4, 1), (4, 1.5), (4, 2)	74.3%	72.4%	50.1%
(4, 2), (4, 2), (4, 2)	74.1%	72.4%	50.1%
(4, 1)	70.8%	69.4%	50.1%
(4, 1), (4, 2)	72.5%	70.2%	50.1%
(4, 1), (4, 2), (4, 4)	<u>74.5%</u>	72.5%	50.1%
(2, 1), (4, 2), (6, 4)	73.6%	72.0%	50.1%
(6, 1), (4, 2), (2, 4)	72.6%	71.7%	50.0%
<b>Sixty-four <math>8 \times 8</math> DCTR kernels</b>			
(4, 1), (4, 1.5), (4, 2)	72.5%	71.4%	50.0%
(4, 2), (4, 2), (4, 2)	72.7%	71.2%	50.1%
(4, 1), (4, 2), (4, 4)	<u>72.9%</u>	71.2%	50.1%
(2, 1), (4, 2), (6, 4)	71.9%	70.2%	50.0%
(6, 1), (4, 2), (2, 4)	71.5%	70.1%	50.1%
<b>Thirty <math>5 \times 5</math> PHARM kernels</b>			
(4, 1), (4, 1.5), (4, 2)	72.0%	70.8%	50.1%
(4, 2), (4, 2), (4, 2)	70.6%	68.8%	50.0%
(4, 1), (4, 2), (4, 4)	<u>72.1%</u>	70.8%	50.1%
(2, 1), (4, 2), (6, 4)	70.3%	68.6%	50.0%
(6, 1), (4, 2), (2, 4)	70.2%	68.7%	50.0%

- basic5000K: The largest-scale dataset used in our experiments. Due to the limitation of machine capacity, relevant experiments are only conducted for stego images with 0.4 bpnzAC (bits per non-zero cover AC DCT coefficient).

Our implementation is based on the publicly available Caffe toolbox [37] with our implemented hand-crafted convolutional layer with DCT basis patterns and Q/T layer according to (8). Our proposed models are trained using mini-batch stochastic gradient descent with “step” learning rate starting from 0.01 and a momentum fixed to 0.9. The batch size in the training procedure is 64 and the maximum number of the iterations is set to 200K.

J-UNIWARD [12], UERD [11] and UED [10], the three state-of-the-art JPEG domain steganographic schemes are our attacking targets in the experiments. The default parameters of the three steganographic schemes are adopted in all of our experiments. 80% cover images are randomly selected from basic50K, basic500K, and basic5000K, respectively. They constitute the training set along with their corresponding stego images. The rest 20% cover-stego pairs in the dataset are for testing. We further guarantee that the cover images included in an arbitrary train set of the three datasets will not appear

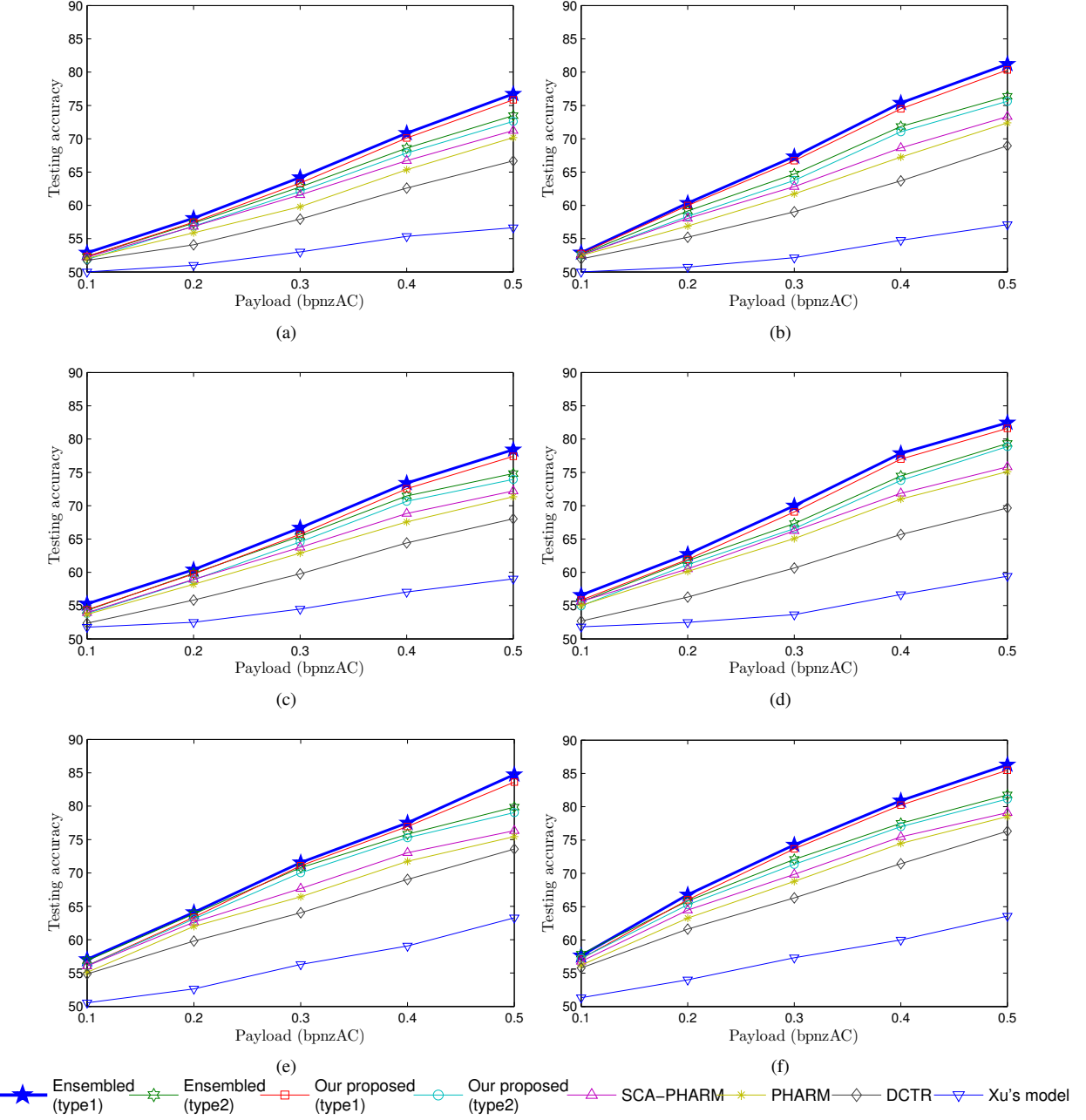


Fig. 3. Comparison of testing accuracy of our proposed frameworks with two subnet configurations and other steganalytic models in the literature, including two hand-crafted JPEG domain rich models (DCTR and PHARM), a selection-channel-aware variant of PHARM (SCA-PHARM) and a deep-learning steganalytic model proposed by Xu et al. [29]. (a) and (b) are the results for J-UNIWARD; (c) and (d) are for UERD; (e) and (f) are for UED. The experiments for (a), (c) and (e) are conducted on basic50K, while those for (b), (d) and (f) are conducted on basic500K.

in all of the three testing sets.

#### B. Impact of the framework structure on the performance

In Tab. I, we compare the effect of different Q/T combinations, different hand-crafted convolutional kernels, and the presence of BN layers. The verification experiments are conducted on basic50K. From Tab. I we can see that under the same conditions, DCTR kernels always perform better than PHARM kernels [23]. The experimental results support our choice that incorporate DCTR kernels in our proposed framework.  $5 \times 5$  DCTR kernels can achieve significant performance

improvement compared to  $3 \times 3$  DCTR kernels. However, the performance of the more complex  $8 \times 8$  DCTR kernels is not even as good as the  $3 \times 3$  DCTR kernels, which indicates that increasing the size of the convolutional kernels cannot always improve the performance of our proposed framework though at the cost of increasing model complexity. Different Q/T combinations also affect the performance of our proposed framework. The combinations with three different quantization steps and the same threshold are of relatively good cost-effectiveness. BN layers in the subnets are crucial to our proposed framework, especially the first one at the bottom

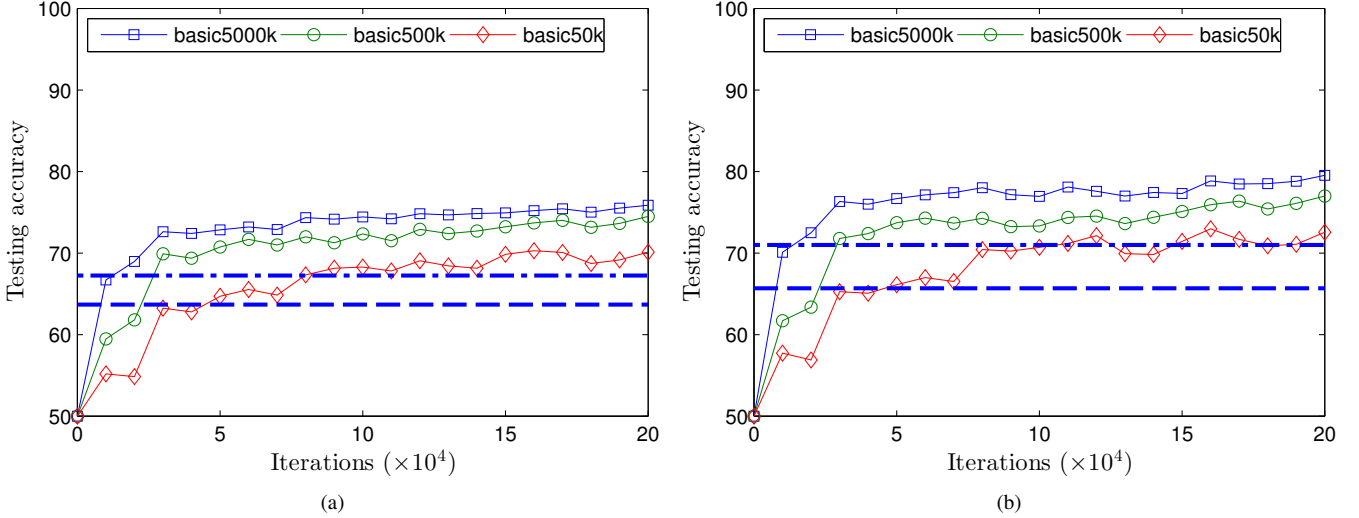


Fig. 4. Testing accuracies versus training iterations for our proposed framework with type1 subnet. The experiments are conducted on basic50K, basic500K and basic5000K, respectively. Only stego images with 0.4bpnzAC are included in the experiments. The dash-dot reference line denotes the best testing accuracy of PHARM, while the dash reference line denotes the best testing accuracy of DCTR in basic500K. (a) For J-UNIWARD steganography. (b) For UERD steganography.

of the subnets. According to results reported in Tab. I, in our final proposed framework, we adopt twenty-five  $5 \times 5$  DCTR kernels,  $T = 4$ ,  $Q = [1, 2, 4]$  and subnet configurations with a BN layer inserted following each convolutional layer.

### C. Comparison to prior art

In Fig. 3, we compare the performance of our proposed frameworks with two subnet configurations and other steganalytic models in the literature. The framework proposed by Xu et al. [29] is referred as Xu's model here. From Fig. 3 we can see that our proposed framework can obtain significant performance improvement compared with DCTR, more advanced PHARM, and even recently proposed selection-channel-aware JPEG rich model SCA-PHARM. Its superiority is more obvious in basic500K. This is due to the fact that with more training samples raised by one magnitude, the large-scale basic500K dataset with 800,000 training samples is more favor of deep-learning frameworks like the one proposed by us. If only consider the performance of a single model, our proposed framework with type1 subnets behaves better than its companion with type2 subnets. Furthermore, the final prediction conducted by the ensembled five independently trained models shows that model ensemble can improve the detection accuracy by 1% regardless of the type of the underlying subnet models. Since the performance of our proposed framework with type1 subnets is always better than that with type2 subnets. We insist on using type1 subnets in the following experiments. On the contrary, for all of the four steganographic algorithms, the performance of Xu's model is poor, whether on small-scale basic50K or on large-scale basic500K.

In Fig. 4, testing accuracies versus training iterations for our proposed framework with type1 subnet are shown when experiments are conducted on basic50K, basic500K and basic5000K, our largest-scale dataset, respectively. The tests

are conducted on standalone testing dataset every  $1 \times 10^4$  iterations and the framework is trained for  $20 \times 10^4$  iterations in total. Only stego images with 0.4bpnzAC are included in the experiments owing to the limitation of machine capacity. Even so for basic5000K there are four million cover-stego pairs, namely eight million images evolved in a training epoch. Our proposed deep-learning framework shows strong learning capacity along with the growth of training samples. From Fig. 4 we can see that the curve of testing accuracy for the framework trained in basic5000K not only is of the best stability one but also is of the best performance. Please also note that  $20 \times 10^4$  iterations is roughly equivalent to 256 epochs for basic50K, 25.6 epochs for basic500K, and only 2.56 epochs for basic5000K. Therefore the great potential of our proposed framework with large-scale training dataset maybe still not completely shown.

### D. Further analysis

In Fig. 5, we observe the attacking-target transfer ability of our proposed framework with type1 subnets. From Fig. 5 we can see that our proposed framework trained with J-UNIWARD stego images and then tested with UERD/UED stego images suffers roughly 3% – 4% detection performance degradation compared with that trained and tested with the same type of stego images. However, the detection performance degradation is acceptable especially for the detection of UED stego images given that UED works in a very different way compared with J-UNIWARD.

$8 \times 8$  block processing during JPEG compression introduces block artifact, which can be used as intrinsic statistical characteristic of JPEG cover images. Secret bits embedded in DCT domain tend to impair block artifact, therefore leaves traces which can be utilized by steganalyzers. One interesting problem is that how much the performance of our proposed framework depends on catching the intrinsic statistical characteristic of block artifact. In Fig. 6, we observe the impact

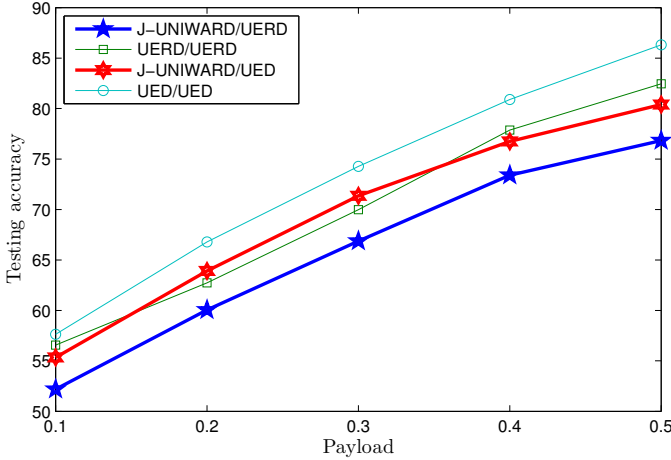


Fig. 5. Comparison of attacking-target transfer ability of our proposed framework. The experiments are conducted on basic500K dataset and our proposed framework with type1 subnets is used. The notations in the legend take the form of the target in training and the target in testing delimited by a slash (/). For example, “J-UNIWARD/UERD” means that J-UNIWARD stego images are used in training while UERD stego images are used in testing.

of altered block artifact on the performance of our proposed framework. The testing set in basic500K contains left-top cropped images in which the original DCT grid alignment is preserved. Now for every testing images in basic500K, their corresponding original ImageNet images are re-compressed with quality factor 75 and then greyed again. their central  $256 \times 256$  regions are cropped to constitute a new testing set. Since central cropping can not preserve the original DCT grid alignment in most cases, as a result the block artifacts in the images of the new testing set are different from those in the training set. However, from Fig. 6 we can see the performance of our proposed model on the new testing set is almost identical with the original testing set in basic500K. The experimental results reveal that the impact of altered block artifact on the performance of our proposed model is small. Our proposed framework has caught more complex intrinsic statistical characteristic besides block artifact.

#### IV. CONCLUDING REMARKS

The application of deep-learning framework in image steganalysis has drawn attention from many researchers in the literature. In this paper we proposed a hybrid deep-learning framework for large-scale JPEG steganalysis. The major contributions of this work are as follows:

- We have proposed a new hybrid deep-learning framework for JPEG steganalysis, which contains a hand-crafted part borrowed from rich models and a learnable part which is composed of a compound deep CNN network.
- As the theoretical basis of the introduction of the hand-crafted part in our proposed model, we proved that the convolutional operation and the Q&T in rich models are not learnable for deep-learning framework.
- We have conducted extensive experiments on large-scale training/testing set extracted from ImageNet. The largest dataset used in our experiments contains ten million

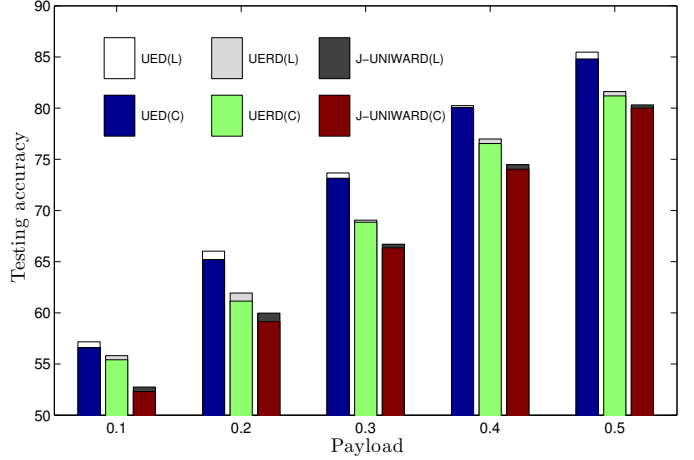


Fig. 6. The impact of altered block artifact on the performance of our proposed framework. In the experiments the target steganography is set to UED, UERD, and J-UNIWARD with 0.4bpnzAC. All of the models are trained on basic500K. In the legend “C” in parentheses denotes the corresponding trained frameworks tested on the central cropped version of basic500K, while “L” in parentheses denotes those trained on the original basic500K. For example, “J-UNIWARD (C)” means that the corresponding framework is trained on the original basic500K and tested on the central cropped version of basic500K.

images, which is three orders of magnitude larger than the common datasets used in the literature.

Our future work will focus on two aspects: (1) more effective deep-learning steganalytic frameworks with higher detection accuracy; (2) further exploration of the application of deep-learning framework on the design of more secure steganography.

#### ACKNOWLEDGMENT

The authors would like to thank DDE Laboratory in SUNY Binghamton for sharing the research codes of steganalysis on the webpage (<http://dde.binghamton.edu/download/>). And specifically, We appreciate Prof. Jiangqun Ni in Sun Yat-sen University, China for permission to use their codes of UED and UERD in our experiments.

#### REFERENCES

- [1] I. Cox, M. Miller, J. Bloom, J. Fridrich, and T. Kalker, *Digital Watermarking and Steganography*, 2nd ed. San Francisco, CA, USA: Morgan Kaufmann Publishers Inc., 2008.
- [2] M. S. Subhedar and V. H. Mankar, “Current status and key issues in image steganography: A survey,” *Computer Science Review*, vol. 13, pp. 95–113, 2014.
- [3] J. Fridrich and T. Filler, “Practical methods for minimizing embedding impact in steganography,” in *Proc. SPIE, Electronic Imaging, Security, Steganography, and Watermarking of Multimedia Contents IX*, vol. 6505, 2007, pp. 650502-1–650502-15.
- [4] T. Pevný, T. Filler, and P. Bas, “Using high-dimensional image models to perform highly undetectable steganography,” in *Proc. 12th Information Hiding Workshop (IH’2010)*, 2010, pp. 161–177.
- [5] V. Holub and J. Fridrich, “Designing steganographic distortion using directional filters,” in *Proc. IEEE 2012 International Workshop on Information Forensic and Security (WIFS’2012)*, 2012, pp. 234–239.
- [6] B. Li, S. Tan, M. Wang, and J. Huang, “Investigation on cost assignment in spatial image steganography,” *IEEE Transactions on Information Forensics and Security*, vol. 9, no. 8, pp. 1264–1277, 2014.
- [7] B. Li, M. Wang, J. Huang, and X. Li, “A new cost function for spatial image steganography,” in *Proc. IEEE 2014 International Conference on Image Processing (ICIP’2014)*, 2014, pp. 4206–4210.

[8] V. Sedighi, J. Fridrich, and R. Cogranne, "Content-adaptive pentary steganography using the multivariate generalized gaussian cover model," in *Proc. SPIE, Media Watermarking, Security, and Forensics 2015*, 2015, pp. 94 090H-1–94 090H-13.

[9] V. Sedighi, R. Cogranne, and J. Fridrich, "Content-adaptive steganography by minimizing statistical detectability," *IEEE Transactions on Information Forensics and Security*, vol. 11, no. 2, pp. 221–234, 2016.

[10] L. Guo, J. Ni, and Y. Q. Shi, "Uniform embedding for efficient JPEG steganography," *IEEE Transactions on Information Forensics and Security*, vol. 9, no. 5, pp. 814–825, 2014.

[11] L. Guo, J. Ni, W. Su, C. Tang, and Y. Q. Shi, "Using statistical image model for JPEG steganography: Uniform embedding revisited," *IEEE Transactions on Information Forensics and Security*, vol. 10, no. 12, pp. 2669–2680, 2015.

[12] V. Holub, J. Fridrich, and T. Denemark, "Universal distortion function for steganography in an arbitrary domain," *EURASIP Journal on Information Security*, vol. 2014, no. 1, pp. 1–13, 2014.

[13] T. Denemark and J. Fridrich, "Improving steganographic security by synchronizing the selection channel," in *Proc. 3rd ACM Information Hiding and Multimedia Security Workshop (IH&MMSec' 15)*, 2015, pp. 5–14.

[14] B. Li, M. Wang, X. Li, S. Tan, and J. Huang, "A strategy of clustering modification directions in spatial image steganography," *IEEE Transactions on Information Forensics and Security*, vol. 10, no. 9, pp. 1905–1917, 2015.

[15] S. Tan and B. Li, "Targeted steganalysis of edge adaptive image steganography based on LSB matching revisited using B-Spline fitting," *IEEE Signal Processing Letters*, vol. 19, no. 6, pp. 336–339, 2012.

[16] X. Li, B. Li, X. Luo, B. Yang, and R. Zhu, "Steganalysis of a PVD-based content adaptive image steganography," *Signal Processing*, vol. 93, no. 9, pp. 2529 – 2538, 2013.

[17] J. Fridrich and J. Kodovský, "Rich models for steganalysis of digital images," *IEEE Transactions on Information Forensics and Security*, vol. 7, no. 3, pp. 868–882, 2012.

[18] W. Tang, H. Li, W. Luo, and J. Huang, "Adaptive steganalysis against WOW embedding algorithm," in *Proc. 2nd ACM Information Hiding and Multimedia Security Workshop (IH&MMSec' 14)*, 2014, pp. 91–96.

[19] T. Denemark, V. Sedighi, V. Holub, R. Cogranne, and J. Fridrich, "Selection-channel-aware rich model for steganalysis of digital images," in *Proc. 6th IEEE International Workshop on Information Forensic and Security (WIFS' 2014)*, 2014, pp. 48–53.

[20] W. Tang, H. Li, W. Luo, and J. Huang, "Adaptive steganalysis based on embedding probabilities of pixels," *IEEE Transactions on Information Forensics and Security*, vol. 11, no. 4, pp. 734–745, 2016.

[21] J. Kodovský and J. Fridrich, "Ensemble classifiers for steganalysis of digital media," *IEEE Transactions on Information Forensics and Security*, vol. 7, no. 2, pp. 432–444, 2012.

[22] V. Holub and J. Fridrich, "Low-complexity features for JPEG steganalysis using undecimated DCT," *IEEE Transactions on Information Forensics and Security*, vol. 10, no. 2, pp. 219–228, 2015.

[23] ———, "Phase-aware projection model for steganalysis of JPEG images," in *Proc. SPIE, Electronic Imaging, Media Watermarking, Security, and Forensics XVII*, vol. 9409, 2015.

[24] T. Denemark, M. Boroumand, and J. Fridrich, "Steganalysis features for content-adaptive JPEG steganography," *IEEE Transactions on Information Forensics and Security*, vol. 11, no. 8, pp. 1736–1746, 2016.

[25] J. Schmidhuber, "Deep learning in neural networks: An overview," *Neural Networks*, vol. 61, pp. 85–117, 2015.

[26] S. Tan and B. Li, "Stacked convolutional auto-encoders for steganalysis of digital images," in *Proc. Asia-Pacific Signal and Information Processing Association Annual Summit and Conference (APSIPA' 2014)*, Dec. 2014.

[27] Y. Qian, J. Dong, W. Wang, and T. Tan, "Deep learning for steganalysis via convolutional neural networks," in *Proc. SPIE, Media Watermarking, Security, and Forensics 2015*, 2015, pp. 94 090J-1–94 090J-10.

[28] L. Pibre, P. Jérôme, D. Ienco, and M. Chaumont, "Deep learning is a good steganalysis tool when embedding key is reused for different images, even if there is a cover source-mismatch," in *Proc. Media Watermarking, Security, and Forensics, Part of IS&T International Symposium on Electronic Imaging (EI'2016)*, Feb. 2016.

[29] G. Xu, H. Z. Wu, and Y. Q. Shi, "Structural design of convolutional neural networks for steganalysis," *IEEE Signal Processing Letters*, vol. 23, no. 5, pp. 708–712, 2016.

[30] ———, "Ensemble of CNNs for steganalysis: An empirical study," in *Proc. 4th ACM Information Hiding and Multimedia Security Workshop (IH&MMSec' 16)*, 2016, pp. 103–107.

[31] P. B. T. Filler and T. Pevný, "Break our steganographic system—the ins and outs of organizing BOSS," in *Proc. 13th Information Hiding Workshop (IH'2011)*, 2011, pp. 59–70.

[32] V. Sedighi, J. Fridrich, and R. Cogranne, "Toss that BOSSbase, Alice!" in *IS&T/SPIE Electronic Imaging (Media Watermarking, Security, and Forensics)*, San Francisco, CA, USA, 14–18 February 2016.

[33] "ImageNet," <http://image-net.org/>, [Online].

[34] "CS231n: Convolutional Neural Networks for Visual Recognition," <http://cs231n.github.io/>, [Online].

[35] C. Szegedy, W. Liu, Y. Jia, P. Sermanet, S. Reed, D. Anguelov, D. Erhan, V. Vanhoucke, and A. Rabinovich, "Going deeper with convolutions," in *Proceedings of the IEEE Conference on Computer Vision and Pattern Recognition*, 2015, pp. 1–9.

[36] S. Ioffe and C. Szegedy, "Batch normalization: Accelerating deep network training by reducing internal covariate shift," *arXiv:1502.03167*, 2015. [Online]. Available: <http://arxiv.org/abs/1502.03167>

[37] Y. Jia, E. Shelhamer, J. Donahue, S. Karayev, J. Long, R. Girshick, S. Guadarrama, and T. Darrell, "Caffe: Convolutional architecture for fast feature embedding," *arXiv:1408.5093*, 2014. [Online]. Available: <http://arxiv.org/abs/1408.5093>